A line confusion limited millimeter survey of Orion KL II. Silicon-bearing species*,**

Belén Tercero¹, Lucie Vincent^{1,2}, José Cernicharo¹, Serena Viti³, and Núria Marcelino^{1,4}

- ¹ Centro de Astrobiología (CSIC-INTA). Departamento de Astrofísica Molecular. Ctra. de Aljalvir Km 4, 28850 Torrejón de Ardoz, Madrid, Spain.
- ² LERMA and UMR 8112 of CNRS, Observatoire de Paris-Meudon, 92195 Meudon Cedex, France.
- Department of Physics and Astronomy, University College London, Gower Street, WC1E 6BT, London, UK.
- National Radio Astronomy Observatory, 520 Edgemont Road, Charlottesville, VA 22903, USA. e-mail: terceromb@cab.inta-csic.es; lucie@damir.iem.csic.es; jcernicharo@cab.inta-csic.es; sv@star.ucl.ac.uk; nmarceli@nrao.edu

Received September 29, 2010; accepted December 3, 2010

ABSTRACT

Context. We present a study of the Silicon-bearing species detected in a line confusion limited survey towards Orion KL performed with the IRAM 30-m telescope.

Aims. The analysis of the line survey is organized by families of molecules. Our aim is to derive physical and chemical conditions for each family taking into account all observed lines from all isotopologues of each species. Due to the large number of transitions in different vibrationally excited states covered by our data, which range from 80 to 280 GHz, we can provide reliable source average column densities (and therefore, isotopologue abundances and vibrational temperatures) for the detected molecules. In addition, we provide a wide study of the physical properties of the source based on the different spectral components found in the emission lines. *Methods.* We have modeled the lines of the detected molecules using a radiative transfer code, which permit us to choose between Large Velocity Gradient (LVG) and Local Thermodinamic Equilibrium (LTE) approximations depending on the physical conditions of the gas. We have used appropriate collisional rates for the LVG calculations. In order to qualitatively investigate the origin of the SiS and SiO emissions in Orion KL we ran a grid of chemical models.

Results. For the v=1 state of SiO we have detected the J=2-1 line and, for the first time in this source, emission in the J=4-3 transition, both of them showing strong masering effect. For SiO v=0, we have detected ²⁸SiO, ²⁹SiO, and ³⁰SiO; in addition, we have mapped the J=5-4 SiO line. For SiS, we have detected the main species, ²⁹SiS, and SiS v=1. Unlikely other species detected in Orion KL (IRc2), the emission peak of SiS appears at a velocity of $\simeq 15.5$ km s⁻¹; a study of the 5-4 SiO line around IRc2 shows this feature as an extended component that probably arises from the interaction of the outflow with the ambient cloud. We derive a SiO/SiS column density ratio of $\simeq 13$ in the plateau component, four times lower than the cosmic O/S ratio $\simeq 48$. In addition, we provide upper limits to the column density of several non-detected Silicon-bearing species. The results of our chemical models show that while it is possible to reproduce SiO in the gas phase (as well as on the grains), SiS is a product of surface reactions, most likely involving direct reactions of Sulphur with Silicon.

Key words. Surveys - Stars: formation - ISM: abundances - ISM: clouds - ISM: molecules - Radio lines: ISM

1. Introduction

The Orion BN/KL (Becklin & Neugebauer, 1967; Kleinmann & Low, 1967) nebula is one of the most studied star formation regions in the Milky Way. At a distance of 414 pc (Menten et al., 2007) the nebula is embedded in a giant molecular cloud harboring practically all phases of the interstellar medium, from hot and diluted plasma, to PDRs, protostellar cores, molecular outflows, SiO and H₂O masering regions, high density cores, intermediate and high mass star formation, protoplanetary disks, and proplydes (see, e.g., Genzel et al., 1980; Genzel & Stuzki, 1989; Wright et al., 1995; Cernicharo et al., 1990, 1994; Plambeck et al., 2009).

Together with Sgr B2, Orion BN/KL nebula exhibits a rich spectrum (see, e.g., Tercero et al., 2010, hereafter Paper I, and references therein) produced by complex organic molecules which are formed through reactions on the grain surfaces during the collapse phase followed by evaporation when radiation from a newly formed star becomes available. Due to the high temperature of the gas, molecular lines are particularly strong in Orion, allowing several line surveys of this source over the last 20 years. Recently, we have performed a line survey towards Orion IRc2 source between 80 and 280 GHz (Paper I), not limited by sensitivity but only by line confusion. The data provide a significant number of transitions for all molecules detected so far towards this source. Although physical structure of the Orion is rather complex, the large number of transitions observed for each species allows to model the different cloud components and to derive reliable physical parameters. In addition, the line survey provides a deep insight on the chemistry of the Orion KL region and allows to refine our knowledge of its chemical structure by searching for new molecular species and

^{*} Appendix A (density diagnostic), Appendix B (online Figures), and Appendix C (online Tables) are only available in electronic form via http://www.edpscience.org

^{**} This work was based on observations carried out with the IRAM 30-meter telescope. IRAM is supported by INSU/CNRS (France), MPG (Germany) and IGN (Spain)

new isotopologues and vibrationally excited states of molecules already known to exist in this source. In a first paper we have presented the line survey and analyzed the CS-bearing species deriving the abundance of CS, OCS, CCS, CCCS, H₂CS, and HCS⁺ (Paper I). In this paper we will analyze the Silicon-bearing species SiO and SiS. SiO has been observed with single dishes and interferometers (see, e.g., Plambeck et al., 2009 and references therein), while only a few observations are available for SiS (Dickinson & Rodríguez-Kuiper, 1981; Ziurys, 1988, 1991).

SiO lines in Orion show a complex pattern of thermal and maser emission. The masers seem to arise from a small region around the radio continuum source I (Churchwell et al., 1987), a young star with a very high luminosity without infrared counterpart, $\simeq 10^5$ L_{\odot}, (Gezari et al., 1998; Greenhill et al., 2004). This source is also driving the low velocity outflow observed in SiO (Beuther et al., 2005; Plambeck et al., 2009) and in other molecular species (Paper I). Recent studies have discussed the driving source of the high velocity outflow: whereas Beuther & Nissen (2008) claimed that SMA1 (a sub-millimeter source not detected at IR and centimeter wavelengths, predicted by de Vicente et al. 2002 and detected by Beuther et al. 2004) is the host of the high velocity outflow (based on combined observations of J=2-1 C¹⁸O from the SMA and the IRAM 30m telescope), Plambeck et al. (2009) defended that this outflow is a continuation of the low velocity outflow (based on CARMA observations of SiO v=0 J=2-1).

The SiO v=1 maser emission was modeled in early interferometric observations as arising from a rotating and expanding disk (Plambeck et al., 1990). However, maser emission was also found in the v=0 J=2-1 line by Wright et al. (1995) adding more complexity to the modeling of the structure of the emitting source. Recently, Goddi et al. (2009) have found maser emission in the v=0 J=1-0 transition of ²⁹SiO and ³⁰SiO associated with source I. In addition, observations of Plambeck et al. (2009) clearly show that the emission of this line arise essentially from an outflow driven by source I. Although our single dish data cannot provide a view of the spatial structure of the thermal and maser emission around that source, the observed maser and thermal lines can provide useful constraint on the physical conditions of the gas.

In addition to the study of SiO and SiS we derive upper limits to the abundance of SiC, SiC_2 , c- SiC_3 , SiC_4 , SiN, SiCN, SiNC, ob- SiC_3 , I- SiC_3 , Si_3 , SiCCO, SiCCS, SiH_2 , H_2CSi , and the different isomers of Si_2H_2 . The observations are described in Sect. 2. The results for SiO and SiS are analyzed in Sect. 3. Section 4 is devoted to the modeling of the observed lines. All these results are discussed in Sect. 5 in terms of comparisons with chemical models predictions for Silicon-bearing species. The effect of the new collisional rates for SiO and SiS is analyzed in the Appendix.

2. Observations and Data Analysis

The observations were carried out using the IRAM 30m radiote-lescope during 2004 September (3 mm and 1.3 mm windows), 2005 March (full 2 mm window), 2005 April (completion of 3 mm and 1.3 mm windows), 2007 January (maps and different positions) and March 2008 (2-D line survey using a multibeam receiver). Four SIS receivers operating at 3, 2, and 1.3 mm were used simultaneously with image sideband rejections within 20-27 dB (3 mm receivers), 12-16 dB (2 mm receivers) and 13 dB (1.3 mm receivers). System temperatures were 100-350 K for the 3 mm receivers, 200-500 K for the 2 mm receivers and 200-800 K for the 1.3 mm receivers, depending on the particu-

Table 1. η_{MB} and HPBW along the covered frequency range

Frequency (GHz)	η_{MB}	HPBW (")
86	0.82	29.0
110	0.79	22.0
145	0.74	17.0
170	0.70	14.5
210	0.62	12.0
235	0.57	10.5
260	0.52	9.5
279	0.48	9.0

Notes. η_{MB} and HPBW along the covered frequency range.

lar frequency, weather conditions, and source elevation. For the spectra between 172-178 GHz, the system temperature was significantly higher, 1000-4000 K, due to proximity of the atmospheric water line at 183.3 GHz. The intensity scale was calibrated using two absorbers at different temperatures and using the Atmospheric Transmission Model (ATM, Cernicharo, 1985; Pardo et al., 2001a). The half power beam width (HPBW) and the main beam efficiency (η_{MB}) along the covered frequency range are given in Table 1.

Pointing and focus were regularly checked on the nearby quasars 0420-014 and 0528+134. The observations were made in the balanced wobbler-switching mode, with a wobbling frequency of 0.5 Hz and a beam throw in azimuth of ± 240 ". No contamination from the off position affected our observations except for a marginal one at the lowest elevations ($\sim 25^\circ$) for molecules having emission along the extended ridge.

The backends used were two filter banks with 512×1 MHz channels and a correlator providing two 512 MHz bandwidths and 1.25 MHz resolution. We pointed towards the (survey) position $\alpha = 5^h \ 35^m \ 14.5^s$, $\delta = -5^\circ \ 22' \ 30.0''$ (J2000.0) corresponding to IRc2.

The spectra shown in the figures are in units of main beam temperature, T_{MB} . In spite of the good image band rejection of the receivers, each setting was repeated at a slightly shifted frequency (10-20 MHz) in order to identify and remove all features arising from the image side band. In the data reduction we have removed most of them above 0.05 K (see Paper I for further explanation of this procedure).

2.1. 2D survey observations

The HERA multibeam receiver was used to carry out a systematic line survey between 216-250 GHz over a region of 144x144" (2x2' approximately) with a 4" spacing. System temperatures were around 400-500 K. The sensitivity of the resulting maps was comparable to those of the pointed line survey with the single pixel SIS receivers. The 2D line survey observations were performed in On-The-Fly mapping mode, with position switching using a emission-free reference position at an offset (-600",0) from IRc2. We used WILMA as the main backend, covering the full 1 GHz bandwidth provided by HERA with 2 MHz of spectral resolution. We also used in parallel the versatile VESPA spectrometer to get some interesting lines within the 1 GHz range with higher spectral resolution (320 kHz), as we did for J=5-4 SiO (from all the 2D survey data only the map of this line is showed in this paper). A full description of the 2D line survey will be published elsewhere (Marcelino et al., in preparation).

3. Results

The line survey has been presented elsewhere (Paper I). This paper is devoted to the study of the emission of Silicon-bearing molecules: we have detected SiO, 29 SiO, 30 SiO, SiO ν =1, SiS, 29 SiS, and SiS ν =1. For Si 18 O and Si 17 O we have evidences of their presence but all their lines in our frequency range are blended with other molecules. We report the detection of the transition J=4-3 of SiO ν =1 for the first time in this source. While this transitions shows strong maser emission, rotational lines for ν ≥2 in the covered frequencies lack of maser emission. In the following subsections we describe the data and the results for each molecular species.

3.1. SiO

Five rotational transitions of silicon monoxide (SiO) fall in the covered frequency range of our line survey. For its isotopologues (²⁹SiO, ³⁰SiO, Si¹⁸O, and Si¹⁷O) and SiO vibrationally excited four rotational transitions are within our frequency range.

The rotational constants used to derive the line parameters have been taken from Sanz et al. (2003) (for SiO, ²⁹SiO, 30 SiO, Si 18 O, SiO ν =1) and for Si 17 O, the line parameters have been derived from the Dunham coefficients, Y_{ij} s, of ²⁸SiO and the isotopic relations Y_{ij} '= Y_{ij} * $(\mu(Si^{17}O)/\mu(SiO))^{(i+2j)/2}$ (where μ is the reduced mass of the isotopologue). The dipole moment (μ =3.098D) was reported by Raymonda et al. (1970). Line parameters and observed intensities for all these lines are given in Table 2. Figure 1 shows the observed lines of SiO and its isotopologues, together with the results from our best model (see Sect. 4.1). Figure 2 shows the SiO v=1 lines within our line survey. The J = 2-1 and J = 4-3 lines show maser emission whereas the J = 5-4 and J = 6-5 are blended with other abundant molecules in Orion and their possible contribution to the observed features is rather weak and two orders of magnitude below the observed emission in the J=2-1 and J=4-3 maser emission. Rotational lines from SiO $v \ge 2$ are below the detection limit of this line survey. Only the v=2 J=2-1 seems to have a very week emission, $T_{MB} \simeq 0.06$ K, at the velocity of the red component of the

The line profiles indicate the contribution to the emerging intensities from different velocity components: the extended and compact molecular ridge (difficult to separate), the hot core, the high velocity outflow, and the low velocity plateau. The latter appears as the most significant contribution to the line profile and intensity.

Table C.1, available electronically only, gives the parameters for the different cloud components derived by fitting several Gaussian profiles to the observed transitions of SiO and to selected lines of ²⁹SiO and ³⁰SiO. The profiles are separated into two components: one wide component which corresponds to the low and high velocity outflows (the plateau), and a narrow one consisting of a mix of the ridge components with the plateau.

The broad component from the plateau dominates the line profiles and hides the contribution of the hot core at 5 km s $^{-1}$, which is only marginally detected as a blue shoulder in the emission from the isotopologues. We interpret this behavior as due to the opacity of the SiO lines in the high velocity gas which could absorb the emission from the hot core (this effect was studied for HDO by Pardo et al. 2001b). However, the line profiles of the 29 SiO and 30 SiO isotopologues, for which the high velocity gas should be thinner, clearly need a component at the velocity of the hot core (see also the discussion for SiS below) in order to reproduce their line profiles.

3.1.1. J=5-4 SiO map

From the 2D survey data of Orion KL, a map of the SiO J=5-4intensity at different velocity ranges is shown in Fig. B.1. The velocity structure of the SiO emission shows the contribution from all the cloud components quoted above. Note the spatial displacement of the emission peak with velocity. Particularly interesting is the spatial distribution of the red and blue wings at the largest velocities (panels top left and bottom right). The high velocity outflow appears as an elliptical shell of gas around IRc2. Recently, Plambeck et al. (2009) have obtained a map with an angular resolution of ≈ 0.5 " of the v=0 J=2-1 line of SiO. Their data for the extreme red velocities, 29-52 kms⁻¹, indicates that the emission is shifted towards the East from source I by 5-10". However, blue extreme velocities, -20 to -40 km s⁻¹, are found several arcseconds W and NW of source I. Wright et al. (1996) obtain a similar result in their aperture synthesis (≃4" resolution) v=0 J=2-1 SiO velocity map of the extreme velocities ($v_{LSR} < -11 \text{ km s}^{-1}$ and $v_{LSR} > 29 \text{ km s}^{-1}$). These results are in very good agreement with our lower angular resolution map. Plambeck et al. (2009) found that the bulk of the emission arises from a bipolar outflow covering velocities from -13 to 16 km s⁻¹, driven by source I and with an extent of $\simeq 6$ " along the NE-SW direction. The large velocity outflow, or extreme velocities, seems to be a continuation of the low velocity outflow but less spatially structured. This "EW bipolarity" of the SiO high velocity outflow was noted already by Olofsson et al. (1981). We have obtained angular source sizes between 16" for the central velocities to 23" for the extreme velocities, assuming emission within the half flux level and corrected for the size of the telescope beam at the observing frequency. The distribution of the high velocity gas is very similar to that found in the extended maser emission of H₂O at 183.3 GHz found by Cernicharo et al. (1990, 1994).

3.2. SiS

Nine transitions of silicon monosulfide 28 Si 32 S ν =0,1 and of its rare isotopologues are present in the covered frequency range. Spectroscopic constants are from Sanz et al. (2003). The dipole moment (μ =1.730D) has been taken from Hoeft et al. (1969). Line frequencies and observational line parameters are given in Table 3. The observed line profiles and the results from our best model (see Sect. 4.2) are shown in Fig. 3, for the main isotopologue, and in Fig. B.2 (for 29 SiS and SiS ν =1). The lines from the other isotopologues are blended with strong lines arising from other molecular species. Only one line (J=9-8 transition) is free of blending for Si 34 S. The line intensities arising from the isotopologues 30 SiS and Si 33 S are below the confusion limit of our line survey.

The line profiles of the most abundant isotopologue display three components: a wide component that corresponds to the plateau, the hot core (clearly seen in the profile of the J=14-13 transition), and a narrower one at $v_{LSR} \simeq 15.5$ km s⁻¹. No emission has been observed from the ridge component. Line parameters are given in Table C.2, available electronically only (in the wide component emission from the plateau and the hot core are merged).

The velocity of the emission peak for the main isotopologue is at $v_{LSR} \approx 15.5 \text{ km s}^{-1}$ which coincides with the LSR velocity of the red component of the SiO v=1 maser emission (which could be a fortuitous agreement, see Sect. 3.2.1). Previous works discuss the presence of SiS in Orion KL and its association

Table 2. Lines of SiO, SiO isotopologues, and SiO vibrationally excited

Molecule	Observed	T_{MB}	$\int T_{MB}dv$	Trasition	Rest	E _u /k	S_{ij}
	v_{LSR} (km s ⁻¹)	(K)	$(K \text{ km s}^{-1})$	J	Frequency (MHz)	(K)	- ,
SiO	11.0	17.5	394±18	2-1	86846.971	6.3	2.00
	8.5	25.6	590±18	3-2	130268.665	12.5	3.00
	8.5	44.6	962±29	4-3	173688.210	20.8	4.00
	7.3	45.0	1485 ± 22	5-4	217104.889	31.3	5.00
	8.0	61.1	2219±43	6-5	260517.985	43.8	6.00
²⁹ SiO	11.5	1.27		2-1	85759.202	6.2	2.00
	11.3	9.22	238±20	4-3	171512.814	20.6	4.00
	15.5^{1}	9.40		5-4	214385.778	30.9	5.00
	10.6^2	12.9		6-5	257255.249	43.2	6.00
³⁰ SiO	14.9^3	1.41		2-1	84746.193	6.1	2.00
	10.1	6.17	108±5	4-3	169486.929	20.3	4.00
	10.6	6.36	140 ± 4	5-4	211853.546	30.5	5.00
	10.0	12.6^{4}	153 ± 14	6-5	254216.751	42.7	6.00
Si ¹⁸ O	6.9^{5}	0.26	•••	2-1	80704.907	5.8	2.00
	8.6	$4.30^{5,6}$	•••	4-3	161404.866	19.4	4.00
	11.2	0.65^{2}		5-4	201751.443	29.0	5.00
	7		•••	6-5	242094.928	40.7	6.00
Si ¹⁷ O	20.4^{8}	0.27		2-1	83588.641	6.0	2.00
	12.3	0.40		4-3	167171.974	20.1	4.00
	12.7	0.71^9		5-4	208959.990	30.1	5.00
	9.2	0.55		6-5	250744.688	42.1	6.00
SiO v = 1	14.2	77.5	587±20	2-1	86243.430	6.2	2.00
	-3.9	113.5	750 ± 19				
	14.0	21.5	123±14	4-3	172481.125	20.7	4.00
	-4.5	4.20					
	10	<1.2	•••	5-4	215596.029	31.0	5.00
	2	<1.2		6-5	258707.350	43.5	6.00

Notes. Emission lines of SiO, SiO isotopologues, and SiO vibrationally excited present in the frequency range of the Orion KL survey. Column 1 indicates the species, Col. 2 gives the observed (centroid) radial velocities, Col. 3 gives the peak line temperature, Col. 4 the integrated intensity, Col. 5 the line transition, Col. 6 the calculated rest frequencies, Col. 7 the energy of the upper level, and Col. 8 gives the line strength.

(1) Blended with 34 SH₂. (2) Blended with CH₃OCOH. (3) Blended with CH₃OH. (4) Blended with CH₃CH₂CN b type. (5) Blended with CH₃CH₂CN in the plane torsion (Tercero et al., in preparation). (6) Blended with CH₂CHCN. (7) Blended with CH₃CH₂CN a type. (8) Blended with H₅₃ β and U line. (9) Blended with CH₃CH₂CN out of plane torsion (Tercero et al., in preparation).

with the SiO *v*=1 maser (Dickinson & Rodríguez-Kuiper, 1981; Sutton et al., 1985; Ziurys, 1988, 1991; Schilke et al., 1997).

Although confusion is large when considering the weak lines of 29 SiS and SiS v=1, we found that their emission peaks at $v_{LSR} \simeq 13.5 \text{ km s}^{-1}$ (see Fig. B.2), a mixture of all cloud components, but dominated by the 15.5 km s⁻¹ feature.

3.2.1. The feature at 15.5 km s^{-1}

At the position of the line survey (IRc2) only SiS (v=0, 1) lines and one component of the SiO maser emission (ν =1) show an intensity peak at 15.5 km s⁻¹. Wright et al. (1990) measured the absolute position of the SiO masers to an accuracy of 0".15 coinciding with the position of radio source I (very close to IRc2). In order to check the origin of this feature we have observed the line profiles of several molecules around IRc2. We have found that the line profiles of SiO show important changes with position. Figure 4 central panel displays a 20" x 20" map centered on IRc2 of the J=5-4 line of SiO; the small panels around the map show the line profile of the J=5-4 transition of SiO at selected positions and show strong differences across the cloud. The intensity peak of SiO lines is at 15.5 km s⁻¹ at the positions $\Delta \alpha$ =-10", $\Delta \delta$ =+6" and $\Delta \alpha$ =-6", $\Delta \delta$ =+14". A comparison of the J=5-4 SiO line at (-10", 6") with the emission of the J=14-13SiS line at (0, 0) is shown in the right panel.

In our map, this extended feature is seen around the position $\Delta\alpha$ =-7", $\Delta\delta$ =+7" (near the BN object) with a radius of \simeq 5 arcseconds. Figure B.3 shows emission lines from different molecules at a position offset (-15", 15") from IRc2. Only molecules with a strong emission from the plateau component (SO, ³⁴SO, SO₂, and SiO) show the 15.5 km s-1 component at this position. Hence, this feature is not a particularity of SiS but arises probably from the interaction of the outflow with the ambient cloud. Consequently, lines toward Orion KL showing a strong intensity and eventually high opacity in the plateau could hide interesting details of other components (hot core, feature at 15.5 km s-1), making line interpretation a very difficult task.

4. Physical parameters of the clouds

Column densities for all detected species have been calculated using an excitation and radiative transfer code developed by J. Cernicharo (Cernicharo 2010, in preparation). Depending on the selected molecule or physical conditions, we assume the large velocity gradient (LVG; Sobolev, 1958; Sobolev, 1960) or local thermodynamic equilibrium (LTE) approximations. Table 4 resume the physical parameters we have obtained for each spectral cloud component from the modeling of SiO and SiS (note that for the new feature at 15.5 km s⁻¹ we have derived the following parameters from the modeling of the SiS lines: T_K =200 K, $n(H_2)$ =5×10⁶ cm⁻³, and $v_{half\ power\ intensity}$ =7.5 km s⁻¹). We as-

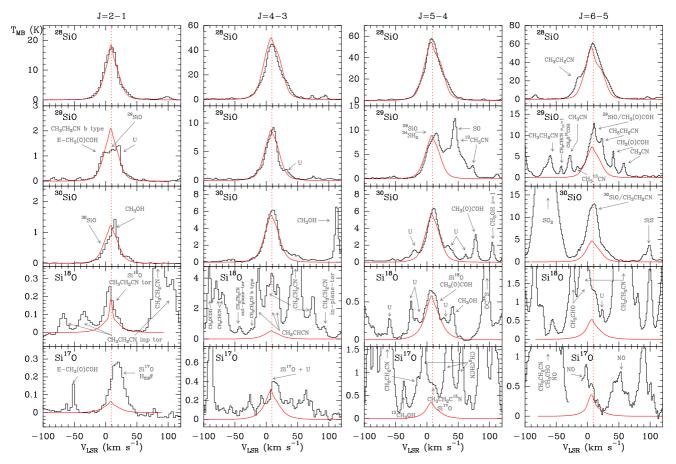


Fig. 1. Observed lines (histogram spectra) and model (thin curves) of SiO and its isotopologues. The dashed line shows a radial velocity at 9 km s⁻¹.

sume uniform physical conditions: kinetic temperature, density, radial velocity, and line width. We adopted these values from the data analysis (Gaussian fits and an attempt to simulate the line widths and intensities with LTE and LVG codes) as representative parameters for the different species. Our modeling also takes into account the size of each component and its offset position with respect to IRc2. Corrections for beam dilution are applied for each line depending on their frequency.

The only free parameter is, therefore, the column density of the corresponding observed species. Taking into account the reduced size of most cloud components the contribution from the error beam is negligible except for the extended ridge which has a small contribution for all observed lines.

In addition to line opacity effects, we discussed other sources of uncertainty in Paper I.

4.1. SiO

LTE conditions have been assumed for the hot core, while LVG calculations have been performed for the extended ridge, compact ridge, plateau, and high velocity plateau, with collisional cross sections of SiO-p-H₂ taken from Dayou & Balança (2006) (see Appendix) for temperatures between 10 K to 300 K including levels up to J = 20 (E_{up}=437 K).

SiO lines appear to be optically thick and therefore the derived SiO column density could be significantly underestimated. The lines of the isotopologues are, however, mostly optically thin so we can estimate the SiO column density assuming standard isotopic abundance ratios $(^{28}\text{Si}/^{29}\text{Si} \approx 20 \text{ and } ^{28}\text{Si}/^{30}\text{Si} \approx 30;$

Anders & Grevesse 1989). The results obtained are shown in Table 5. Due to the weakness of the less abundant isotopologues lines (Si¹⁸O and Si¹⁷O) and large line overlap problems, we can only obtain upper limits for their column density. We have estimated the uncertainty between 20-30 % for the ²⁹SiO and ³⁰SiO results.

The cloud component with the largest column density corresponds to the plateau with $N(\mathrm{SiO})_{plateau} = (4.7\pm1.0)\times10^{15}~\mathrm{cm}^{-2}$; while the total column density of SiO is $N(\mathrm{SiO})=(7.4\pm2.0)\times10^{15}~\mathrm{cm}^{-2}$, both results in agreement with those obtained from the line survey of Orion using the Odin satellite (Persson et al., 2007). Our study provides a column density between six times to one order of magnitude larger than that obtained in the surveys at high frequency by Schilke et al. (2001) and Comito et al. (2005). Larger column densities have been reported by Ziurys & Friberg (1987) and Wright et al. (1996), while Johansson et al. (1984) and Sutton et al. (1995) obtained a beam average column density in good agreement with our results. These differences are mostly due to the different assumptions on the physical conditions and cloud structure made in the interpretation of the observations.

We derive a column density $^{29}\text{SiO}/^{30}\text{SiO}$ ratio of 2, 2, 1.7, 1.4, 1.25 for the extended ridge, compact ridge, plateau, high velocity plateau, and hot core, respectively, in agreement with the standard solar value of $^{29}\text{Si}/^{30}\text{Si} \simeq 1.5$ (Anders & Grevesse, 1989). We can estimate a lower limit for the isotopic ratio $^{16}\text{O}/^{18}\text{O}$ and an estimation of $^{18}\text{O}/^{17}\text{O}$ by means of the total column density ratios $N(\text{Si}^{16}\text{O})/N(\text{Si}^{18}\text{O}) \gtrsim 239$ and $N(\text{Si}^{18}\text{O})/N(\text{Si}^{17}\text{O}) \simeq 2$ with large uncertainty due to the severe blending of their lines with other species. These values are

Table 3. Lines of SiS, 29 SiS, and SiS v=1

Molecule	Observed	T_{MB}	$\int T_{MB}dv$	Trasition	Rest	E _u /k	S_{ij}
	v_{LSR} (km s ⁻¹)	(K)	$(K \text{ km s}^{-1})$	J	Frequency (MHz)	(K)	
SiS	12.5	0.29	6.1±0.3	5-4	90771.558	13.1	5.00
	16.7	0.53	11.5 ± 0.5	6-5	108924.294	18.3	6.00
	15.5	1.34	30 ± 1	8-7	145227.045	31.4	8.00
	16.5	2.14^{1}	43±1	9-8	163376.773	39.2	9.00
	16.2	2.42		11-10	199672.219	57.5	11.00
	11.1	3.10		12-11	217817.651	68.0	12.00
	8.9^{2}	20.0		13-12	235961.363	79.3	13.00
	17.7	4.45		14-13	254103.213	91.5	14.00
	15.2	4.25		15-14	272243.058	104.5	15.00
²⁹ SiS	16.6	0.019		5-4	89103.781	12.8	5.00
	3			6-5	106923.019	18.0	6.00
	16.1	0.087		8-7	142558.873	30.8	8.00
	4			9-8	160375.213	38.5	9.00
	5			12-11	213816.228	66.7	12.00
	13.1	0.25		13-12	231626.772	77.8	13.00
	6			14-13	249435.521	89.8	14.00
	12.9	0.24		15-14	267242.338	102.6	15.00
SiS $v=1$	noise level			5-4	90329.891	13.0	5.00
	2			6-5	108394.292	18.2	6.00
	12.4	0.12		8-7	144520.370	31.2	8.00
	13.3	0.46^{7}		9-8	162581.760	39.0	9.00
	11.9	0.17		11-10	198700.526	57.2	11.00
	8			12-11	216757.615	67.6	12.00
	14.8	0.31		13-12	234812.983	78.9	13.00
	13.8	0.36		14-13	252866.487	91.0	14.00
	1	•••	•••	15-14	270917.984	104.0	15.00

Notes. Emission lines of SiS, ²⁹SiS, and SiS v=1 present in the frequency range of the Orion KL survey. Column 1 gives the species, Col. 2 the observed (centroid) radial velocities, Col. 3 gives the peak line temperature, Col. 4 the integrated intensity, Col. 5 the line transition, Col. 6 the calculated rest frequencies, Col. 7 the energy of the upper level, and Col. 8 gives the line strength.

(1) Blended with CH_3OCOH . (2) Blended with $^{13}CH_3OH$. (3) Blended with U line. (4) Blended with $(CH_3)_2CO$. (5) Blended with $^{34}SO_2$. (6) Blended with CH_3OH . (7) Blended with $^{33}SO_2$. (8) Blended with CH_3CH_2CN b type.

Table 4. Physical parameters of Orion KL components

Parameter	Extended ridge	Compact ridge	Plateau	High velocity plateau	Hot core	15.5 km s ⁻¹ component
Source diameter (")	120	15	30	30	10	10
Offset (IRc2) (")	0	7	0	0	2	5
$n(H_2)$ (cm ⁻³)	1.0×10^5	1.0×10^6	1.0×10^{6}	1.0×10^6	5.0×10^7	5.0×10^6
$T_K(K)$	60	110	125	125	225	200
v _{half power intensity} (km s ⁻¹)	4	4	25	50	10	7.5
v_{LSR} (km s ⁻¹)	9	7.5	9	9	5.5	15.5

Notes. Obtained physical parameters for Orion KL.

Table 5. Column densities - SiO

Species	Extended ridge	Compact ridge	Plateau	High velocity plateau	Hot core
	$N \times 10^{15} \text{ (cm}^{-2})$				
SiO from ²⁹ SiO	0.04±0.01	0.20±0.05	5.0±1.0	1.4±0.4	1.0±0.3
SiO from 30SiO	0.03 ± 0.007	0.15 ± 0.04	4.5 ± 1.0	1.5 ± 0.4	1.2 ± 0.3
SiO (Average)	0.035 ± 0.009	0.17 ± 0.05	4.7 ± 1.0	1.4 ± 0.4	1.1 ± 0.3
²⁹ SiO	0.0020 ± 0.0005	0.010 ± 0.003	0.25 ± 0.06	0.07 ± 0.02	0.05 ± 0.02
³⁰ SiO	0.0010 ± 0.0003	0.005 ± 0.002	0.15 ± 0.04	0.05 ± 0.02	0.04 ± 0.01
Si ¹⁸ O	≲0.0005	≲0.0005	≲0.01	≲0.01	≲0.01
Si ¹⁷ O	≲0.0001	≲0.0005	≲0.005	≲0.005	≲0.005

Notes. Column densities of the different SiO isotopologues calculated with LVG and LTE codes.

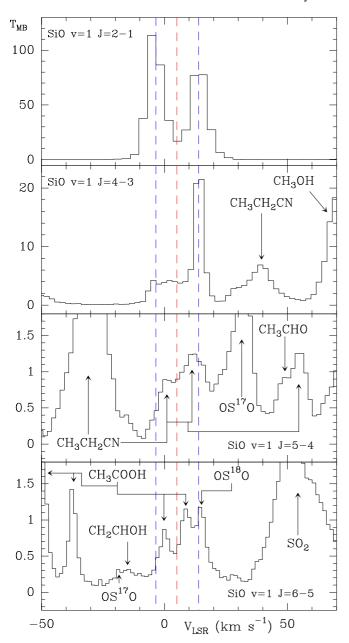


Fig. 2. Observed lines of vibrationally excited SiO v = 1 showing maser emission in the transitions J = 2-1 and J = 4-3. The dashed lines show radial velocities at at -3.4, +5.1 and +13.9 km s⁻¹.

two times lower than those of the solar system. In Paper I we derived $N(^{16}\text{OCS})/N(^{18}\text{OCS}) = 250\pm135$, while Persson et al. (2007) obtained a $^{18}\text{O}/^{17}\text{O}$ ratio of 3.6 from $\text{C}^{18}\text{O}/\text{C}^{17}\text{O}$.

We have also modeled the 5-4 SiO line in the offset position (-10",6") from IRc2 (see Fig. 4) in order to provide a column density for the 15.5 km s⁻¹ feature. Using the same column densities obtained above for the different components, we have added the feature at 15.5 km s⁻¹ with a column density of $(1.0\pm0.3)\times10^{15}$ cm⁻².

4.1.1. SiO maser lines

SiO maser emission in Orion was discovered by Snyder & Buhl (1974) through its v=1 J=2-1 transition. Plambeck et al. (1990) suggested that the emission arises from an expanding rotating disk around IRc2. The emission from this line, studied by several authors, has been found to be confined to a region

of 20-100 AU (3-10×10¹⁴ cm) around the radiocontinuum source I (Churchwell et al., 1987) and to trace a protostellar wind and/or outflow expanding with a velocity $\simeq 20 \text{ kms}^{-1}$ (Plambeck et al., 1990; Menten & Reid, 1995; Greenhill et al., Doeleman et al., 1999; Plambeck et al., Doeleman et al., 2004: Greenhill et al., 2004: Matthews et al., 2007). Source I has not an infrared counterpart in the range 4-22 μm (Greenhill et al., 2004), suggesting that it is surrounded by a dusty disk producing severe extinction. Source I is placed between Orion IRc2 and the hot core and excites the masers of SiO and H₂O (Genzel & Stuzki, 1989; Plambeck et al., 1995). Several other lines of SiO in v=1 and 2 have been searched towards this source an some of them have been detected (v=1J=1-0, J=2-1, J=3-2; see references above). The v=1 J=4-3line was searched without success by Schwartz et al. (1982). In our line survey we have covered the J=2-1, 4-3, 5-4, and 6-5 lines of all vibrational states of SiO. As shown in Fig. 2, only

the v=1 J=2-1 and 4-3 transitions have been unambiguously detected (the J=4-3 for the first time). For the rotational lines of the v=2 level the range of velocities covered by the SiO v=1 J=2-1 maser is always contaminated by other lines. The v=2 J=2-1 line shows a weak feature coincident with the red emission at 15 km s⁻¹ but it arises from the $4_{2,3}-3_{1,2}$ line of E-CH₃OCOH as confirmed from the observed intensities of other lines of this species. The v=2 J=4-3 line shows a strong feature at the velocity of the blue component of the maser but it arises from (CH₃)₂CO. The other lines from v=2, 3, and 4 are always blended with other lines. In our survey we have covered the same rotational and vibrational quantum numbers of the SiO isotopologues. None of them shows any maser effect within the sensitivity of our observations.

The observation of several ro-vibrational lines of SiO can be used to constraint the physical properties of the gas at spatial scales from a few tens to a few hundred AU from the source. Goddi et al. (2009) have modeled the emission of several isotopologues of SiO. They conclude that while the v=0 J=1-0maser emission arises from a region with radius >100 AU and densities $<10^7$ cm⁻³, the v=1,2 J=1-0 and J=2-1 are produced in a region of ~100 AU around source I. Our observed intensity ratio v=1 J=2-1/J=4-3 is $\approx 5-10$ depending on the velocity component. We obtain such a behavior for column densities of $\simeq 10^{19}$ cm⁻² and densities $\simeq 10^8$ cm⁻³. For higher densities the ratio increases and the predicted intensities of the J=2-1 and J=4-3 lines, although large, are not compatible with the inferred brightness temperatures which could be well above 10⁵ K. We have run several models with different physical parameters. Our results suggest that the gas responsible for maser emission could have densities up to 10^8 cm⁻³, sizes of 100 AU, and gas temperatures around 600-800 K, a factor two below those of Goddi et al. (2009). With these parameters for the emitting region the abundance of SiO should be as high as 10^{-4} .

González-Alfonso & Cernicharo (1997) have shown that the masers of SiO and their isotopologues are affected by line overlap in the infrared between themselves. Such overlaps seem to have little effects on the emission of SiO, 29 SiO, and 30 SiO in $v\neq 0$ for which maser emission has been found in evolved stars (Cernicharo et al., 1991b; González-Alfonso et al., 1996).

4.2. SiS

In the same way as for SiO, LTE conditions have been assumed for the hot core, while LVG calculations have been performed for the 15.5 km s⁻¹ feature and the plateau, with collisional cross sections SiS-o-H₂ for 41 levels and $5 < T_k < 300$ K taken from Klos & Lique (2008) (see Appendix). The fits are shown in Figs. 3 and B.2. The column density results are shown in Table 6. We have estimated the uncertainty to be about 20-30 % for the results of SiS and 50 % for ²⁹SiS and SiS ν =1. Our largest value of the column density for SiS corresponds to the feature at 15.5 km s⁻¹ obtaining $N(\text{SiS})_{15.5 \text{ kms}^{-1} \text{ feature}} = (7.0\pm1.7) \times 10^{14} \text{ cm}^{-2}$; the total column density for SiS is $N(\text{SiS})_{total} = (1.35\pm0.40) \times 10^{15} \text{ cm}^{-2}$. A similar value was obtained by Ziurys (1988) and Ziurys (1991) whereas Dickinson & Rodríguez-Kuiper (1981) found $N(\text{SiS}) = (1-2) \times 10^{13} \text{ cm}^{-2}$.

Assuming that SiS emission is optically thin, as indicated by our calculations, we derive an isotopic abundance of $^{28}\text{Si}/^{29}\text{Si} \approx 14$, 35, and 30 for the 15.5 feature, the plateau, and the hot core, respectively *i. e.* close to the solar system value. We provide an average value of $^{28}\text{Si}/^{29}\text{Si} = 26 \pm 10$.

The N(SiO)/N(SiS) column density ratio observed in the plateau is ≈ 13 , in good agreement with

Dickinson & Rodríguez-Kuiper (1981) and four times lower than the cosmic O/S ratio of 48 (Anders & Grevesse, 1989). Ziurys (1991) found a N(SiO)/N(SiS) ratio \approx 40-80. We can also derive this ratio by means of $N(^{29}SiO)/N(^{29}SiS)$, obtaining a value $\simeq 25$ for the plateau. In order to compare column density ratios, we have to assume that the region of the line formation is the same for each molecule and the excitation temperature is similar for both species, for that reason we only provide this ratio for the plateau component. In the previous work of this line survey (Paper I), we derived O/S ratios using different species/families of molecules: N(HCO⁺)/N(HCS⁺) $\simeq 13$, $N(H_2CO)/N(H_2CS) \simeq 12$, and $N(CO)/N(CS) \simeq 370$; in addition, Persson et al. (2007) found $N(H_2O)/N(H_2S) \simeq 20$ and $N(H_2CO)/N(H_2CS) \simeq 15$. All the obtained values, but $N(CO)/N(CS) \simeq 370$, show a similar O/S ratio, indicating that the different formation paths of different molecules maintain a constant ratio O/S in the same particular region of the cloud.

¿From the column density obtained for SiS in the ground and the vibrationally excited states, it is easy to estimate a vibrational temperature by means of:

$$\frac{exp\left(-\frac{E_{v=x}}{T_{vib}}\right)}{f_{v}} = \frac{N(SiS \quad v=x)}{N(SiS)} \tag{1}$$

where E_{v_x} is the excitation energy of the vibrational state ($E_{v=1} = 1077 \text{ K}$, T_{vib} is the vibrational temperature, f_v is the vibrational partition function, N(SiS v = x) is the column density of the vibrational state and N(SiS) is the column density of SiS in the ground state. The vibrational partition function can be approximated by

$$f_{\nu} = 1 + exp\left(-\frac{E_{\nu_3}}{T_{vib}}\right) +$$

$$+2exp\left(-\frac{E_{\nu_2}}{T_{vib}}\right) + exp\left(-\frac{E_{\nu_1}}{T_{vib}}\right)$$
(2)

which, for low T_{vib} leads to $f_v \simeq 1$.

We obtain $T_{vib} = 500\pm200$ K in the 15.5 km s⁻¹ component. This value is higher than the kinetic temperature we have assumed for that component (200 K). This result could indicate an inner and hotter emitting region for vibrationally excited SiS, suggesting that the excitation temperature varies across the feature at 15.5 km s⁻¹. In Paper I we calculated the vibrational temperature in the hot core component for OCS $v_2 = 1$ and $v_3 = 1$ obtaining \approx 210 K and an upper limit of 300 K for CS v = 1. As we have indicated in our previous paper, all these results could point to radiative pumping effects in the populations of the vibrationally excited states of these molecules (taking into account the magnitude of the collisional rates of these species).

Higher angular resolution observations are necessary to resolve any possible excitation gradient and temperature profile in the feature at 15.5 km s^{-1} and in the hot core component.

4.3. Other Silicon-bearing Molecules

We provide upper limits for the column density of several Silicon molecules not detected in our line survey. We have assumed the four typical spectroscopic components of Orion KL (hot core, extended ridge, compact ridge, and plateau) plus the 15.5 feature, and a LTE approximation for all these molecules. Table 7 shows the results obtained, the dipole moment of each species, and references for the spectroscopic constants.

SiC.- Millar (1980) predicted SiC to be an abundant form of Silicon in dense clouds on basis of gas phase chemistry models.

Table 6. Column densities - SiS

Species	15.5 km s ⁻¹ Component N ×10 ¹⁴ (cm ⁻²)	Plateau N×10 ¹⁴ (cm ⁻²)	Hot core N $\times 10^{14}$ (cm ⁻²)
SiS	7.0±1.7	3.5 ± 0.8	3.0±0.7
²⁹ SiS	0.50 ± 0.25	0.10 ± 0.05	0.10 ± 0.05
SiS $v=1$	0.80 ± 0.40	0.20 ± 0.10	0.20 ± 0.10

Notes. Column densities of different SiS species calculated with LVG and LTE codes.

Table 7. Column density upper limits

Molecule	Column density	Dipole	References
	$\lesssim N \times 10^{14} \text{ (cm}^{-2})$	moment (D)	spectroscopic constants
SiC	1.3	1.600^{1}	(2)
SiC_2	0.35	2.393^3	(4)
c-SiC ₃	0.13	4.200^5	(6)
SiC_4	0.04	6.420^7	(8)
SiN	0.61	2.560^9	(10)
SiCN	0.31	2.900^{11}	(12)
SiNC	0.31	2.000^{11}	(12)
ob-SiC ₃	0.16	2.200^{5}	(13)
1-SiC3	0.04	4.800^{14}	(14)
Si_3	4	0.350^{15}	(16)
SiCCO	0.40	1.937^{17}	(18)
SiCCS	0.65	1.488^{19}	(19)
o-SiH ₂	13	0.075^{20}	(21)
o-H ₂ CSi	1.7	0.300^{22}	(22)
p-H ₂ CSi	1.4	0.300^{22}	(22)
mb-Si ₂ H ₂	0.34	μ_a =0.962/ μ_b =0.039 ²³	(24)
o -db- Si_2H_2	2.5	$\mu_c = 0.480^{25}$	(25)

Notes. Upper limits for the column density of non-detected Silicon-bearing molecules in Orion KL.

(1) Langhoff & Bauschlicher (1990); (2) Cernicharo et al. (1989) and Bogey et al. (1990); (3) Suenram et al. (1989); (4) Gottlieb et al. (1989) and Suenram et al. (1989); (5) Alberts et al. (1990); (6) Apponi et al. (1999b); (7) Gordon et al. (2000); (8) Ohishi et al. (1989) and Gordon et al. (2000); (9) Kerkines & Mavridis (2005); (10) Saito et al. (1983) and Bizzocchi et al. (2006); (11) Apponi et al. (2000); (12) Apponi et al. (2000) and McCarthy et al. (2001); (13) McCarthy et al. (1999); (14) McCarthy et al. (2000); (15) Vasiliev et al. (1997); (16) McCarthy & Thaddeus (2003a); (17) Botschwina (2005); (18) Sanz et al. (2005); (19) Botschwina et al. (2002); (20) Gabriel (1993); (21) Hirota & Ishikawa (1999); (22) Izuha et al. (1996); (23) Grev & Schaefer III (1992); (24) Cordonnier et al. (1992) and McCarthy & Thaddeus (2003b); (25) Bogey et al. (1994).

This molecule has been detected by Cernicharo et al. (1989) towards the envelope of the red giant star IRC+101216, but not in Orion (see Schilke et al., 1997 for the attempts of detection in this source). We have obtained an upper limit for its total column density of 1.3×10^{14} cm⁻² providing an abundance ratio of $N(\text{SiO})/N(\text{SiC}) \gtrsim 57$.

 SiC_2 .- We have not detected silicon dicarbide in our line survey. Turner (1991) reported the detection of this molecule in the hot core of Orion KL. However, this result is quite uncertain due to the few observed transitions (three) and their weakness. We have searched for other lines of SiC_2 in our line survey and we conclude that the intensities of the lines from this molecule are below the confusion limit as many of these lines are blended or missing. We obtain an upper limit to its column density of 3.5×10^{13} cm⁻² and an abundance ratio $N(SiO)/N(SiC_2)\gtrsim211$. This molecule and its isotopologues have also been detected towards IRC+101216 by Thaddeus et al. (1984) (SiC₂), Cernicharo et al. (1986) ($^{29}SiC_2$ and $^{30}SiC_2$) and Cernicharo et al. (1991a) (Si¹³CC).

 $c\text{-}SiC_3$.- Apponi et al. (1999a) detected rhomboidal SiC₃ in the expanding envelope of the evolved carbon star IRC+10216. For this molecule we have calculated an upper limit to its column density in Orion KL of 1.3×10^{13} cm⁻², and a ratio $N(\text{SiO})/N(\text{SiC}_3)\gtrsim570$.

 SiC_4 .- SiC_4 was first detected in the space by Ohishi et al. (1989) in the envelope of IRC+10216. For this molecule we have calculated an upper limit to its column density in Orion KL of 3.5×10^{12} cm⁻², and a ratio $N(SiO)/N(SiC_4) \gtrsim 2114$.

SiN.- Silicon nitride has been detected in IRC+10216 by Turner et al. (1992) and in the galactic center cloud SgrB2(M) by Schilke et al. (2003). We have not found SiN above the confusion limit in Orion; note, however, that some U-lines in our survey could be assigned to SiN (see Fig. B.4, panels 1, 6 and 9) but we consider that the evidences for its presence in Orion are not strong enough within the coverage of our survey. We provide an upper limit of 6.1×10^{13} cm⁻², and $N(SiO)/N(SiN) \gtrsim 121$.

SiCN.- Cyanosilylidyne was identified in spectra recorded toward IRC+10216 by Guélin et al. (2000). The calculated upper limit to its column density in Orion KL is 3.1×10^{13} cm⁻², deriving the ratio $N(\text{SiO})/N(\text{SiCN}) \gtrsim 240$.

SiNC.- The isocyanosilylidyne isomer has a thermodynamic stability very similar to that of SiCN, but a slightly smaller dipole moment. It was detected toward IRC+10216 by Guélin et al. (2004). We provide an upper limit of 3.1×10^{13} cm⁻² to its column density, and a ratio $N(\text{SiO})/N(\text{SiNC}) \gtrsim 240$.

SiH, SiH₄.- In our frequency range there are not transitions of SiH, a molecule tentatively detected by Schilke et al. (2001) towards Orion KL, so we cannot assess that detection. The other

Silicon molecule detected in the space (in IRC+10216) is SiH_4 (Golhaber & Betz, 1984), but this molecule can be only observed at IR wavelengths.

 $ob\text{-}SiC_3$, l-SiC3, Si_3 , SiCCO, SiCCS, $o\text{-}SiH_2$, $o\text{-}H_2CSi$, $p\text{-}H_2CSi$, $mb\text{-}Si_2H_2$, $o\text{-}db\text{-}Si_2H_2$.- These molecules have not been detected in the space yet. Upper limits for their column density are shown in Table 7.

5. Discussion

SiO is a key tracer of shocked emission. Many interferometric observations show that thermal and maser SiO emission depicted the low velocity outflow centered in source I in Orion KL (Blake et al., 1996; Wright et al., 1996; Beuther et al., 2005; Plambeck et al., 2009; Goddi et al., 2009; Zapata et al., 2009). In addition, SiO traces many other molecular outflows in different sources (Jiménez-Serra et al., 2004; Gibb et al., 2007; De Buizer et al., 2009; Zapata et al., 2009). Mookerjea et al. (2007) have not found emission from SiO at the position of the hot molecular core in G34.26+0.15. This hot core does not have a central source but rather it is externally heated, similar to the Orion compact ridge, by shocks, ionization fronts and stellar winds. Mookerjea et al. (2007) pointed out that the lack of SiO in this hot core rules out any significant role played by shocks in determining the hot core chemistry. Observations of SiO in the L1448-mm outflow permit to distinguish between the shock precursor and the postshock components (Jiménez-Serra et al., 2005); they observed an enhancement in the abundances of SiO (and another shock tracers) by one order of magnitude in the shock precursor component and three orders of magnitude in the postshock gas (leading to the broadening of the line profiles), evidence of recent ejection of SiO from grains (Flower et al., 1996).

5.1. Molecular abundances

Molecular abundances were derived using the H2 column density calculated by means of the $C^{18}O$ column density (1.5×10¹⁶, 1.5×10^{16} , 1×10^{17} , 5×10^{16} cm⁻², and 2×10^{17} cm⁻² for the extended ridge, compact ridge, plateau, high velocity plateau, and hot core, respectively) and the isotopic abundance ${}^{16}O/{}^{18}O=250$, both provided in Paper I, assuming that CO is a robust tracer of H_2 and therefore their abundance ratio is roughly constant, ranging from $CO/H_2 \simeq 5 \times 10^{-5}$ (for the ridge components) to 2×10^{-4} (for the hot core and the plateau). In spite of the large uncertainty in this calculation, we include it as a more intuitive result for the molecules described in the paper. We obtained $N(H_2) = 7.5 \times 10^{22}$, 7.5×10^{22} , 2.1×10^{23} , 6.2×10^{22} , and 4.2×10^{23} cm⁻² for the extended ridge, compact ridge, plateau, high velocity plateau, and hot core, respectively; for the 15.5 km s⁻¹ component we assume $N(H_2)=1.0\times10^{23}$ cm⁻² as an average value in Orion KL. In addition, we assume that the H₂ column density spatially coincides with the emission from the species considered. Our estimated source average abundances for each Orion KL component are summarized in Table C.3 (only available online), together with comparison values from other authors (Sutton et al. 1995, Persson et al. 2007, and Ziurys 1988). The differences between the abundances shown in Table C.3 are mostly due to the different H₂ column density considered, to the assumed cloud component of the molecular emission and discrepancies in the sizes of these components.

5.2. On the origin of the SiO and SiS emission

In order to qualitatively investigate the origin of the SiS and SiO emissions in Orion KL we ran a grid of models using the chemical model UCL_CHEM (Viti et al., 2004a,b; Lerate et al., 2010), a time and depth dependent gas-grain model.

We modeled the hot core and the plateau separately. Both models are two phase calculation. In Phase I we follow the chemical and dynamical evolution of a collapsing core up to a final density of 5×10^7 cm⁻³ for the hot core component and 10^6 cm⁻³ for the plateau component as derived in Sect. 4. The initial gas is at typical densities of $\sim 200 \text{ cm}^{-3}$ and in atomic form (apart from a fraction of hydrogen which is already in molecular form) and it undergoes a free-fall collapse (Rawlings et al., 1992) until the final densities are reached. During this time, atoms and molecules from the gas freeze on to the dust grains and they hydrogenate where possible. Note that the advantage of this approach is that the ice composition is not assumed but it is derived by a time dependent computation of the chemical evolution of the gas/dust interaction process. However, the ice composition does depend on the percentage of gas depleted on to the grains during the collapse, and this in turns depend on the density as well as on the sticking coefficient and other properties of the species and of the grains (see Rawlings et al. 1992). In our model we can vary such percentage (reflecting the uncertainty on the grain properties and sticking probabilities) and the degree (or efficiency) of depletion (as well as the viability of different surface reactions) is explored in this study. Our initial elemental abundances for Phase I are as in Bell et al. (2006) (see Table 1). We also ran some models where the initial abundances of both S and Si were either depleted or enhanced by a factor of 10 with respect to these values, reflecting the uncertainty of their degree of depletion onto dust. In Phase II, we follow the chemical evolution of the remnant core. For the hot core models, we simulate the effect of the presence of an infrared source in the center of the core or in its vicinity by subjecting the core to an increase in gas and dust temperature, up to T = 300 K. This increasing of temperature is based on the luminosity of the protostar by using the observational luminosity function of Molinari et al. (2000). The models we use have been published before: for the models describing the hot core we refer the reader to Viti et al. (2004a) and Lerate et al. (2010) while for the models describing the plateau we refer the reader to Lerate et al. (2008), Lerate et al. (2010) and Viti et al. (2004b). In both models the presence of a non dissociative C-shock (modeled as in Bergin et al. 1997) can be simulated. If a shock is included in the model then sputtering also occurs and is faster than thermal evaporation. We have ran a total of 6 models for the hot core component and 2 models for the plateau component. For the hot core model we investigated the sensitivity of the chemical abundances to the degree of gas depleted on to the grains during the formation of the core; the branching ratios of surface reactions relevant to the formation of SiO and SiS; the initial abundances of Sulphur and Silicon; whether the gas is subjected to a non-dissociative shock during the hot core lifetime. For the plateau models, we only varied the initial Sulphur and Silicon abundances.

We were able to reproduce the observed column density of SiO with most models. The only constrain we found was that the temperature of the gas must be at least $\sim 100~K$ or, alternatively, must have undergone a shock. SiS, on the other hand, is difficult to produce: surface reactions (and subsequent evaporation or sputtering of the mantles) seem to be necessary. We find that the only models that succeed in reproducing the data are those where a percentage (even as small as 5%) of Sulphur on

the grains react with Si to form SiS: Figure 5 shows the column density of SiO and SiS as a function of time during Phase II of the hot core for models differing only in the mantle formation efficiency of SiS (i.e on how efficient Si bonds with Sulfur). A qualitative match with the observation can be achieved, at early times, by those models where only 5%-10% of Sulphur on the grains react with Si to form SiS, or at late times if a higher percentage of Sulphur is involved in the formation of SiS.

Note, however, that exact ages can not be derived from these considerations as the relationship of the time dependencies with the efficiency of SiS formation on grains will depend on the desorption times of SiO and SiS.

In conclusions, while it is possible to reproduce SiO in the gas phase (as well as on the grains), our models indicate that SiS is a product of surface reactions, most likely involving direct reactions of Sulphur with Silicon.

6. Summary

In Paper I we presented a line survey of Orion KL taken with the 30m IRAM telescope. The sensitivity achieved allows to perform a line confusion limited survey. Due to the wide frequency range covered and data quality we decided to present the line survey in a series of papers focused in different molecular families. In this paper we presented the study of the emission from Silicon-bearing species, SiO and SiS, as well as their isotopologues and their vibrationally excited states.

For the v=1 state of SiO we have detected the J=2-1 line and, for the first time in this source, emission in the J=4-3 transition, both of them showing strong masering effect. The well known components of Orion (hot core, plateau, high velocity plateau, extended ridge, and compact ridge) contribute to the observed emission from SiO and its isotopologues whereas for SiS, 29 SiS, and SiS v=1 we have found emission from the hot core, the plateau, and a feature at 15.5 km s⁻¹. In order to check the origin of this feature we have observed the line profiles of J=5-4 SiO around IRc2 and of different molecules at an offset position (-15", 15") from IRc2. We conclude that this extended feature is seen around the position $\Delta \alpha = -7$ ", $\Delta \delta = +7$ " (near the BN object) with a radius of ≈ 5 arcseconds and probably arises from the interaction of the outflow with the ambient cloud.

The physical parameters obtained for each Orion KL component are in agreement with those we can find in the Orion literature. For the feature at $v_{LSR}=15.5~{\rm km~s^{-1}}$ we derive T_K =200 K, $n(H_2)$ =5×10⁶ cm⁻³, and $v_{half~power~intensity}$ =7.5 km s⁻¹. Column densities have been calculated with radiative transfer codes based on either the LVG or the LTE approximations taking into account the physical structure of the source and using the new SiO-p-H₂ and SiS-o-H₂ collisional rates. The results are provided as source averaged column densities. In this way, we obtain a total column density of $(7.4\pm2.0)\times10^{15}$ and $(1.35\pm0.40)\times10^{15}~{\rm cm^{-2}}$ for SiO and SiS, respectively.

We have derived several column density ratios which permit us to provide the following average isotopic abundances: ${}^{28}\text{Si}/{}^{29}\text{Si} = 26 \pm 10$, ${}^{29}\text{Si}/{}^{30}\text{Si} = 1.7 \pm 0.6$, ${}^{16}\text{O}/{}^{18}\text{O} \gtrsim 239$, ${}^{18}\text{O}/{}^{17}\text{O} \simeq 2$. We have also investigated the origin of the SiS and SiO emission in Orion KL by the use of a gas-grain chemical model and find that while SiO can be easily formed in the gas phase, SiS seems to be a product of grain surface reactions, most likely involving direct reactions of Sulphur with Silicon.

The resulting vibrational temperature for SiS ν =1 in the feature at 15.5 km s⁻¹ is \simeq 500 K, larger than the kinetic temperature derived for this component indicating an IR pumping or

a warmer component difficult to see in the lines of the ground vibrational state.

Finally, we have derived upper limits for the column density of non-detected molecules (Silicon-bearing species). For the detected species in other sources SiC, SiC₂, c-SiC₃, SiC₄, SiN, SiCN, and SiNC the upper limits for their column density are $1.3\times10^{14},\ 3.5\times10^{13},\ 1.3\times10^{13},\ 3.5\times10^{12},\ 6.1\times10^{13},\ 3.1\times10^{13},\ and\ 3.1\times10^{13}\ cm^{-2}$, respectively.

Acknowledgements. We thank the Spanish MEC for funding support through grants AYA2003-2785, AYA2006-14876, AYA2009-07304, ESP2004-665 and AP2003-4619 (M. A.), Consolider project CSD2009-00038 the DGU of the Madrid Community government for support under IV-PRICIT project S-0505/ESP-0237 (ASTROCAM).

References

Alberts, I. L., Grev, R. S. & Schaefer III, H. F. 1990, J. Chem. Phys., 93, 5046 Anders, E. & Grevesse, N. 1989 GeCoA, 53, 197

Andreazza, C. M. and Marinho, E. P. 2007, MNRAS, 380, 365

Apponi, A. J., McCarthy, M. C., Gottlieb, C. A. & Thaddeus, P. 1999 ApJ, 516

Apponi, A. J., McCarthy, M. C., Gottlieb, C. A. & Thaddeus, P. 1999, J. Chem. Phys., 111, 3911

Apponi, A. J., McCarthy, M. C., Gottlieb, C. A. & Thaddeus, P. 2000, ApJ, 536L, 55

Bell, T. A., Roueff, E., Viti, S., Williams, D. A. 2006, MNRAS, 371, 1865

Becklin, E. E. & Neugebauer, G. 1967, ApJ, 147, 799 Bergin, E. A., Goldsmith, P. F., Snell, R. L., & Langer, W. D. 1997, ApJ, 482,

285

Beuther, H., Zhang, Q., Greenhill, L. J. et al. 2004, ApJ, 616L, 31 Beuther, H., Zhang, Q., Greenhill, L. J., et al. 2005, ApJ, 632, 355

Beuther, H., Zhang, Q., Greenhill, L. J., et al. 2005, ApJ, 632, 35. Beuther, H. & Nissen, H. D. 2008 ApJ, 679L, 121

Bieniek, R. J. and Green, S. 1983, ApJ, 265, L29

Bizzocchi, L., Degli Esposti, C. & Dore, L. 2006, A&A, 455, 1161

Blake, G. A., Mundy, L. G., Carlstrom, J. E., Padin, S., Scott, S. L., Scoville, N. Z. and Woody, D. P. 1996, ApJ, 472, L49

Bogey, M., Demuynck, C. & Destombes, J. L. 1990, A&A, 232L, 19

Bogey, M., Bolvin, H., Cordonnier, M., et al. 1994, J. Chem. Phys., 100, 8614

Botschwina, P., Sanz, M. E., McCarthy, M. C. & Thaddeus, P. 2002, J. Chem. Phys., 116, 10719

Botschwina, P. 2005, JMoSt: THEOCHEM, 724, 95

Cernicharo, J. 1985. Internal IRAM report (Granada: IRAM)

Cernicharo, J., Kahane, C., Gómez-Gonzalez, J. & Guélin, M. 1986, A&A, 167L, 9

Cernicharo, J., Gottlieb, C. A., Guelin, M., Thaddeus, P. & Vrtilek, J. M. 1989, ApJ, 341L, 25

Cernicharo, J., Thum, C., Hein, H., John, D., Garcia, P., Mattioco, F., 1990, A.&A., 231, L15

Cernicharo, J., Guélin, M., Kahane, C., Bogey, M. & Demuynck, C. 1991, A&A, 246, 213

Cernicharo, J., Bujarrabal, V. & Lucas, R. 1991, A&A, 249L, 27

Cernicharo, J., González-Alfonso, E., Alcolea, J., Bachiller, R., John, D., 1994, ApJ, 432, L59

Cernicharo, J., Guélin, M., Kahane, C., 2000, A&A Supl. Series, 142, 181

Churchwell, E., Felli, M., Wood, D.O.D., Massi, M-, 1987, ApJ, 321, 516

Comito, C., Schilke, P., Philips, T. G., Lis, D. C., Motte, F. and Mehringer, D. 2005 ApJS, 165, 127

Cordonnier, M., Bogey, M., Demuynck, C. & Destombes, J.-L. 1992, J. Chem. Phys., 97, 7984

Dayou, F. and Balança, C. 2006, A&A, 459, 297

De Buizer, J. M., Redman, R. O., Longmore, S. N., Caswell, J. & Feldman, P. A. 2009, A&A, 493, 127

de Vicente, P., Martín-Pintado, J., Neri, R. & Rodríguez-Franco, A. 2002 ApJ, 574L, 163

Dickinson, D. F. & Rodríguez-Kuiper, E. 1981, ApJ, 247, 112

Doeleman, S.S., Lonsdale, C.J., Pelkey, S., 1999, ApJ, 510, L55

Doeleman, S. S., Lonsdale, C. J., Kondratko, P. T., Predmore, C. R. 2004, ApJ, 607, 361

Flower, D. R., Pineau des Forets, G., Field, D. & May, P. W. 1996, MNRAS, 280, 447

Gabriel, W. 1993, CP, 174, 45

Genzel, R., Downes, D., Schwartz, P.R., Spencer, J.H., Pankonin, V., & Baars, J., 1980, ApJ, 239, 519

Genzel, R., & Stuzki, J., 1989, ApJ, 574, 258

```
Gezari, D.Y., Backman, D.E., & Werner, M.W., 1998, ApJ, 509, 283
Gibb, A. G., Davis, C. J. & Moore, T. J. T. 2007, MNRAS, 382, 1213
Goddi, C., Greenhill, L. J., Chandler, C. J., et al. 2009, ApJ, 698, 1165
Goldhaber, D. M. & Betz, A. L. 1984, ApJ, 279L, 55
```

González-Alfonso, E., Alcolea, J. & Cernicharo, J. 1996, A&A, 313L, 13

González-Alfonso, E. & Cernicharo, J. 1997, A&A, 322, 938

Gordon, V. D., Nathan, E. S., Apponi, A. J., et al. 2000, J. Chem. Phys., 113, 5311

Gottlieb, C. A., Vrtilek, J. M. & Thaddeus, P. 1989, ApJ, 343L, 29

Green, S., and Chapman, S. 1978, ApJS, 37, 169

Greenhill, L.J., Gwinn, C.R., Schwartz, C., Moran, J.M., Diamond, P.J., 1998, Nature, 396, 650

Greenhill, L. J., Gezari, D. Y., Danchi, W. C., Najita, J., Monnier, J. D., & Tuthill, P. G. 2004, ApJ, 605, L57

Grev, R. S. & Schaefer III, H. F. 1992, J. Chem. Phys., 97, 7990

Guélin, M., Muller, S., Cernicharo, J., et al. 2000, A&A, 363L, 9

Guélin, M., Muller, S., Cernicharo, J., McCarthy, M. C. & Thaddeus, P. 2004, A&A, 426L, 49

Hirota, E. & Ishikawa, H. 1999, J. Chem. Phys., 110, 4254

Hoeft, J., Lovas, F. J., Tiemann, E. & Törring, T. 1969, ZNatA, 24, 1422

Izuha, M., Yamamoto, S. & Saito, S. 1996, J. Chem. Phys., 105, 4923

Jiménez-Serra, I., Martń-Pintado, J., Rodríguez-Franco, A. & Marcelino, N. 2004, ApJ, 603L, 49

Jiménez-Serra, I., Martín-Pintado, J. & Rodríguez-Franco, A. 2005 ApJ, 627, L121

Johansson, L. E. B., Andersson, C., Elldér, J., Friberg, P., Hjalmarson, Å., Hölglund, B., Irvine, W. M., Olofsson, H. & Rydbeck, G. 1984 A&A, 130, 227

Kerkines, I. S. K. & Mavridis, A. 2005, J. Chem. Phys., 123, 14301

Kleinmann, D. E. & Low, F. J. 1967, ApJ, 149L, 1

Klos, J. & Lique, F., 2008, MNRAS, 390 239

Langhoff, S. R. & Bauschlicher, C. W., Jr. 1990, J. Chem. Phys., 93, 42L

Lerate, M. R., Yates, J., Viti, S., et al. 2008, MNRAS, 387, 1660L

Lerate, M. R., Yatesi J., Barlow, M. J., Viti, S., Swinyard, B. M. 2010, MNRAS, 406, 2445L

Lique, F., Tobola, R., Klos, J., Feautrier, N., Spielfiedel, A., Vincent, L., Chalasiński, G., and Alexander, M. H. 2008, A&A, 478, 567

Matthews, L. D., Goddi, C., Greenhill, L. J., Chandler, C. J., Reid, M. J., & Humphreys, E. M. L. 2007, in IAU Symp. 242, Astrophysical Masers and their Environments, ed. J. M. Chapman & W. A. Baan (Dordrecht: Kluwer), 130

McCarthy, M. C., Apponi, A. J. & Thaddeus, P. 1999, J. Chem. Phys., 111, 7175McCarthy, M. C., Apponi, A. J., Gottlieb, C. A. & Thaddeus, P. 2000, ApJ, 538, 766

McCarthy, M. C., Apponi, A. J., Gottlieb, C. A. & Thaddeus, P. 2001, J. Chem. Phys., 115, 870

McCarthy, M. C. & Thaddeus, P. 2003, ApJ, 592L, 91

McCarthy, M. C. & Thaddeus, P. 2003, JMoSp, 222, 248

Menten, K.M., Reid, M.J., 1995, ApJ, 445, L157

Menten, K.M., Reid, M.J., Forbricl, J., Brunthaler, A., 2007, ApJ, 474, 515 Millar, T., J. 1980 Ap&SS 72, 509M

Molinari, S., Brand, J., Cesaroni, R., & Palla, F. 2000, A&A, 355, 617

Mookerjea, B., Casper, E., Mundy, L. G. & Looney, L. W., 2007, ApJ, 659, 447

Ohishi, M., Kaifu, N., Kawaguchi, K., et al. 1989, ApJ, 345L, 83

Olofsson, H., Hjalmarson, A. & Rydbeck, O. E. H. 1981, A&A, 100L, 30

Pardo, J. R., Cernicharo, J. and Serabyn, E. 2001, IEEE Tras. Antennas and Propagation, 49, 12

Pardo, J. R., Cernicharo, J., Herpin, F., et al. 2001, ApJ, 562, 799

Persson, C. M., Olofsson, A. O. H., Koning, N., et al. 2007, A&A 476, 807

Plambeck, R.L., Wright, M.C.H., Carlstrom, J.E., 1990, ApJ, 348, L65

Plambeck, R.L., Wright, M.C.H., Mundy, L.G., & Looney, L.W., 1995, ApJ, 502, L75

Plambeck, R.L., Wright, M.C.H., Rao, R., 2003, ApJ, 594, 911

Plambeck, R.L., Wright, M.C.H., Friedel, et al., 2009, ApJ, 704, L25

Raymonda, J. W., Muenter, J. S. & Klemperer, W. A. 1970, J. Chem. Phys., 52, 3458

Rawlings, J. M. C., Hartquist, T. W., Menten, K. M., & Williams, D. A. 1992, MNRAS, 255, 471

Saito, S., Endo, Y. & Hirota, E. 1983, J. Chem. Phys., 78, 6447

Sanz, M. E., McCarthy, M. C. and Thaddeus, 2003, P. J. Chem. Phys., 119, v22, 11715

Sanz, M. E., Alonso, J. L., Blanco, S. Lesarri, A. & Lpez, J. C. 2005, ApJ, 621L, 157

Schilke, P., Groesbeck, T. D., Blake, G. A. & Philips, T. G. 1997 ApJS, 108, 301Schilke, P., Benford, C. J., Hunter, T. R., Lis, D. C. & Philips, T. G. 2001 ApJS, 132, 281

Schilke, P., Leurini, S., Menten, K. M. & Alcolea, J. 2003 A&A, 412, 15 Schwartz, P.R., Zuckerman, B., Bologna, J.M., 1982, ApJ, 256, L55

Snyder, L.E., & Buhl, D., 1974, ApJ, 189, L31

Sobolev, V. V. 1958, en "Theorical Astrophysics". ed. Ambartsumyan, Pergamon Press Ltd. London Cap. 29

Sobolev, V. V. 1960, en "Moving Envelopes of Stars". Hardward University Press

Suenram, R. D., Lovas, F. J. & Matsumura, K. 1989, ApJ, 342L, 103

Sutton, E. C., Blake, G. A., Masson, C. R. & Philips, T. G. 1985 ApJS, 58, 341
Sutton, E. C., Peng, R., Danchi, W. C., Jaminet, P. A., Sandell, G. & Russell, P. G. 1995 ApJS, 97, 455

Tercero, B., Pardo, J. R., Cernicharo, and Goicoechea, J. R. submitted to A.&A. Thaddeus, P., Cummins, S. E. & Linke, R. A. 1984 ApJ, 283, 45

Turner, B. E. 1991 ApJS, 76, 617

Turner, B. E., Chan, K.-W., Green, S., and Lubowich, D. A. 1992, ApJ, 399, 114 Vasiliev, I., Ögüt, S. & Chelikowsky, J. R. 1997, PhRvL, 78, 4805

Vincent, L., Lique, F., Spielfiedel, A., and Feautrier, N. 2007, A&A, 472, 1037 Viti, S., Codella, C., Benedettini, M., & Bachiller, R. 2004, MNRAS, 350, 1029 Viti, S., Collings, M. P., Dever, J. W., McCoustra, M. R. S. & Williams, D. A. 2004, MNRAS, 354, 1141

Wright, M. C. H., Carlstrom, J. E., Plambeck, R. L. and Welch, W. J. 1990 AJ, 99, 1299

Wright, M. C. H., Plambeck, R. L., Mundy, L.G., Looney, L.W., 1995 ApJ, 455, L185

Wright, M. C. H., Plambeck, R. L. and Wilner, D. J. 1996 ApJ, 469, 216

Zapata, L. A., Menten, K. Reid, M. & Beuther, H. 2009, ApJ, 691, 332

Ziurys, L. M. and Friberg, P. 1987 ApJ, 314, L49

Ziurys, L. M. 1988, ApJ, 324, 544 Ziurys, L. M. 1991, ApJ, 379, 260

List of Objects

'Orion KL' on page 1

'IRc2' on page 1

'source I' on page 2

'SMA1' on page 2

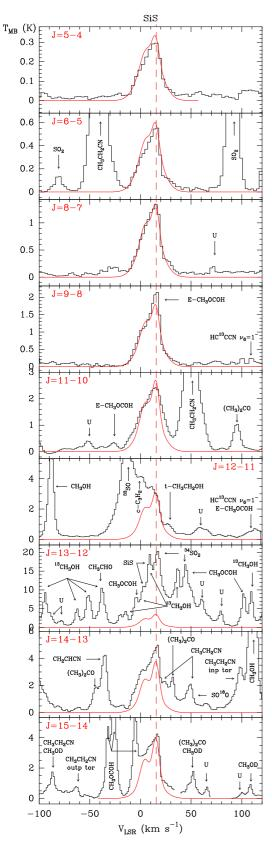


Fig. 3. Observed lines (histogram spectra) and model (thin curves) of SiS. The dashed line shows a radial velocity at 15.5 km s⁻¹.

B. Tercero et al.: Survey towards Orion KL: Silicon bearing species

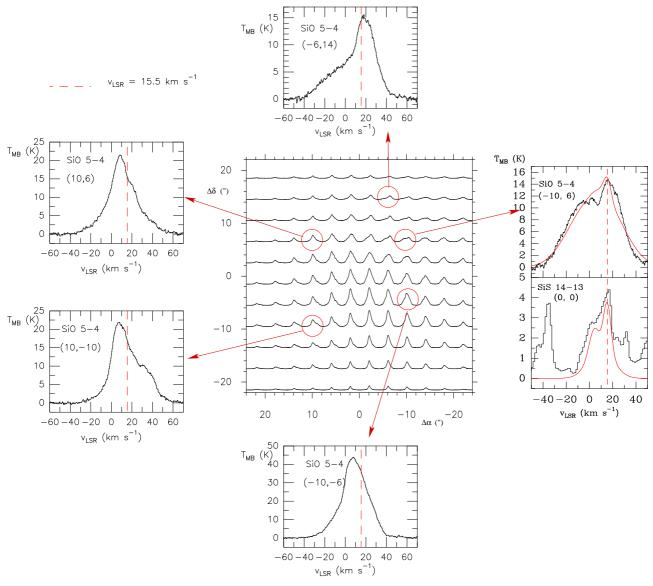


Fig. 4. Central panel shows a 20" x 20" map, centered at IRc2, of the J=5-4 line of SiO; the *right panel* shows a comparison between the J=5-4 line at an offset (-10",6"), and the SiS J=14-13 line towards IRc2, and the resulting model for each line (thin curves). The *rest of the panels* show the SiO J=5-4 line at different positions.

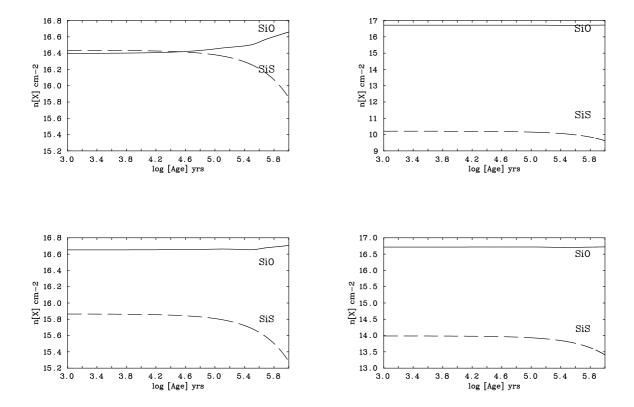


Fig. 5. Column densities of SiO (solid line) and SiS (dotted line) as a function of time from Phase II of the hot core model with an initial elemental abundance of $1x10^{-6}$ for Sulphur and $8x10^{-8}$ for Silicon. The different plots show different efficiencies for the formation of SiS on the grain, namely: 100% (top left); 0% (top right); 30% (bottom left); 10% (bottom right).

Appendix A: Density diagnostic

In this section we study the influence of collisional rates on the modelling of the SiO and SiS lines observed in our line survey of Orion. Although most of the emission in Orion arises from regions of high volume density, the intensity of the high velocity wings apparent in the SiO and SiS line profiles arise from a region, the plateau, in which the density is not enough to thermalize the rotational levels of high dipole moment molecules such as SiO (3.1 D) and SiS (1.73 D). Hence, collisional rates are needed for each species to derive the physical conditions. For SiO previous calculations by Green and collaborators (Bieniek & Green, 1983; Turner et al., 1992; see http://www.giss.nasa.gov/data/mcrates#sio) have provided collisional rates for this molecule and temperatures 20-1500 K. These collisional rates have been recalculated using a new SiO-p-H₂ surface by Dayou & Balança (2006). However, no collisional rates were available of SiS until recently: Vincent et al. (2007) and Klos & Lique (2008) have calculated the state to state collisional rates for the system SiS-He and SiS-H₂, respectively.

We have tested the influence of collisional rates on the modelling of the SiO and SiS lines observed in our line survey of Orion. Using the recent rates quoted above we have computed line intensity ratios between some transitions to provide tools to estimate the physical conditions in astrophysical sources. We have covered volumne densities between 10^2 - 10^9 cm⁻³ and kinetic temperatures from 10 to 300 K including levels up to J=20 and J=40 for SiO and SiS, respectively. In the following we will analyse the excitation conditions for $1\rightarrow0$, $2\rightarrow1$, $3\rightarrow2$, $5\rightarrow4$, $12\rightarrow11$, and $19\rightarrow18$ for both molecules.

A.1. SiO

The line intensity ratios for SiO are shown in Figs. A.1 (kinetic temperature between 10 and 100 K) and A.2 (for a temperature of 300 K). In Fig. A.1 we can notice that the intensity ratio $T_B(3\rightarrow 2)/T_B(2\rightarrow 1)$ is particularly sensitive to densities of about 10^4 to 10^6 cm⁻³, whereas for $T_B(5\rightarrow 4)/T_B(1\rightarrow 0)$ it shows important variations in the density range 10^6 to 10^7 cm⁻³. Using the intensity ratio $T_B(5\rightarrow 4)/T_B(12\rightarrow 11)$, we can explore density values around 10^7 -5×10⁸ cm⁻³. For T_K =300 K, and $T_B(12\rightarrow 11)/T_B(19\rightarrow 18)$, we can trace densities above 10^5 cm⁻³, as seen in Fig. A.2. For lower densities the 19-18 line will be very weak.

To illustrate this point, we deduce from our observations the intensity ratio $T_B(2\rightarrow 1)/T_B(3\rightarrow 2)$ of SiO, and find $\simeq 2.6$ (see Table 2), which corresponds, depending on the column density and for $T_K=100$ K, to densities between $10^{5.5}$ and 10^7 cm⁻³. Our results for the physical parameters of the different cloud components discussed in previous sections are given in Table 4.

The collisional rates calculated by Turner et al. (1992) have been used in the past to describe collisions of SiO molecules with H_2 . We have used through the paper the new rates of Dayou & Balança (2006). As a first step in modelling SiO emission in warm clouds we have made a comparison between the results using both sets of collisional rates for a large range of physical conditions: T_K =10-300 K, N(SiO)=10¹²-10¹⁵ cm⁻², and $n(H_2)$ =1-10⁹ cm⁻³. Figure A.3 shows the brightness temperature (T_B) ratio (predictions using the Dayou & Balança, 2006 rates over those obtained from Turner et al., 1992 rates) as a function of H_2 density for different values of the SiO column density and temperature and for the six first transitions of this molecule. The plots in Fig. A.3 show that the difference in the predicted line intensities between both sets of collisional rates

never exceed 40% (J=6-5 line), being always below 20% for all other rotational lines and kinetic temperatures. The lowest temperature for the collisional rates of Turner et al. (1992) is 20 K; we have extrapolated these rates to obtain the corresponding ones at 10 K. For most transitions the predicted line intensities from the Dayou & Balança (2006) rates are lower than those predicted from Turner et al. (1992) rates for densities below $\simeq 10^5$ cm⁻³. Although the differences in line intensities are not significant for the determination of the physical properties of the emitting gas in interstellar clouds, we have adopted in our SiO calculations the new rates of Dayou & Balança (2006).

A.2. SiS

We have performed the same study for SiS using the rates calculated by Vincent et al. (2007). Figs. A.4 and A.5 show our results. We observe the same trends as for SiO, but for lower densities. Thus, the $T_B(3\rightarrow 2)/T_B(2\rightarrow 1)$ ratio increases in the density range 10^3 to 10^5 cm $^{-3}$, the second one $T_B(5\rightarrow 4)/T_B(1\rightarrow 0)$ in 10^4 to 10^5 cm $^{-3}$, and the last graphs of Fig. A.4 show that $T_B(5\rightarrow 4)/T_B(12\rightarrow 11)$ vary mostly between 10^5 and a few 10^6 cm $^{-3}$. In Fig. A.5, we can see that for $T_K=300$ K, $T_B(12\rightarrow 11)/T_B(19\rightarrow 18)$ are useful for densities around 10^5 cm $^{-3}$. Two of those lines have been detected in our survey, the transitions $5\rightarrow 4$ and $12\rightarrow 11$, with an intensity ratio of $\simeq 0.12$. For $T_K=100$ K we can derive a volume density $\simeq 10^{5.5}$ cm $^{-3}$.

Before 2007, no collisional data was available for SiS. Hence most authors have adopted the SiO collisional rates for SiS. As quoted above, the system SiS-He has been studied by Vincent et al. (2007) and Lique et al. (2008) have compared these rates with the correspondings for the SiS-H₂ system. They have shown that, when scaled by the square root of the collision reduced mass, the SiS-He rates were a reasonable approximation to describe collisions with H₂. We have updated the LVG code by adding the new SiS-He and SiS-H₂ rates. We have calculated the line intensities and compared the results to those obtained with rates for SiO from Turner et al. (1992) (multiplied by a factor 2 to take into account the larger geometrical size of the SiS molecule). Figure A.6 shows the line intensity ratio (brightness temperature obtained with rates from Vincent et al., 2007 over those calculated with rates from Turner et al., 1992) as a function of n(H₂) for the six first rotational transitions. The discrepancies in the line intensities between the two cases do not exceed 50%. As for SiO, we can notice that the differencies between the two sets of collisional rates are the same for all column densities: the line intensity predicted with rates for SiS are lower than those predicted from Turner et al. (1992) rates for densities up to $\approx 10^3$. These differences are quite small and do not affect the determination of the physical parameters performed by authors that have used previously the Turner et al. (1992) rates in their models to interpret SiS observations. We tried also to describe SiS excitation by collisions with the rate coefficients for the system CS-He from Green & Chapman (1978) with an appropriate scaling factor. The predicted intensities show a reasonable agreement with those derived from SiS-He or SiS-H₂ collisional rates. These results show that with the actual calibration accuracy for the SiS observations, the determination of the properties of the emitting gas is not very sensitive to small differences in collisional rates. It is a rather curious result that the predicted line intensities with both sets of collisional rates, deduced from two different potential energy surfaces, moreover, with different propensity rules, produce similar intensity ratios (when the scaling factor is adequately selected). In the determination of the SiS column densities we have used the SiS-H₂ rates (Klos & Lique, 2008) al-

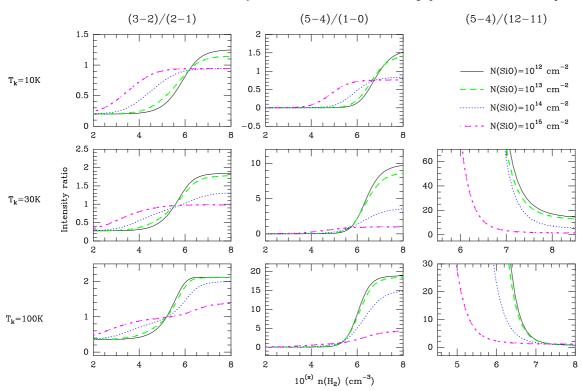


Fig. A.1. Intensity ratio between two transitions for SiO as a function of H_2 density with the SiO column densities equal to 10^{12} , 10^{13} , 10^{14} and 10^{15} cm⁻² and temperatures from 10 K to 100 K.

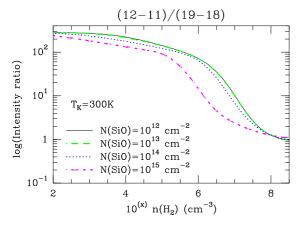


Fig. A.2. Same as A.1 but for T = 300 K.

though no significant differences are found when we used the SiS-He ones.

In order to better quantify the effects of the use of scaled SiO-He rates in predicting SiS intensities, we have considered a case in which the lines are optically thin, for instance, $n(H_2)=10^5$ cm⁻³, $T_K=40$ K and $N(SiS)=3.10^{12}$ cm⁻². The predicted line intensities from SiS-He rates are $T_B(2\rightarrow 1, 4\rightarrow 3, 6\rightarrow 5)=0.08, 0.26, 0.33$ K. To obtain these results from scaled SiO-He rates we need a density of 7.10^4 cm⁻³ or to reduce the scaling factor from 2 to ≈ 1.5 , i.e., an error lower than 2 in density.

We have compared predictions from the SiS-He rates with those obtained from the SiS-H₂ rates and we have found not significant variation between both.

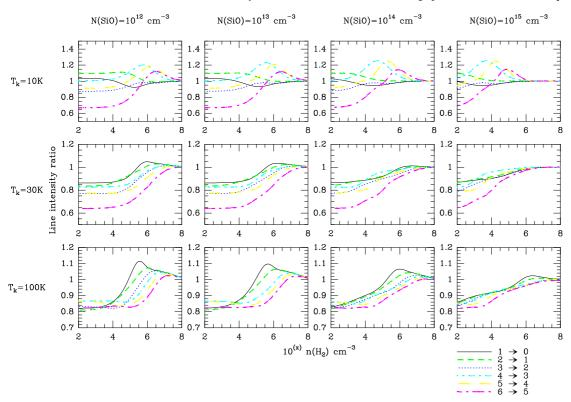


Fig. A.3. Comparison of the line intensities predicted using two different sets of collisional rates (see text) for different lines, column densities and densities.

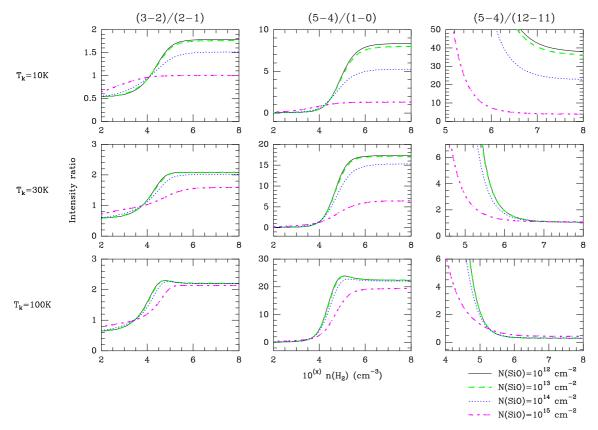


Fig. A.4. Intensity ratio between two transitions for SiS as a function of H_2 density with the SiS column density equal to 10^{12} , 10^{13} , 10^{14} and 10^{15} cm⁻².

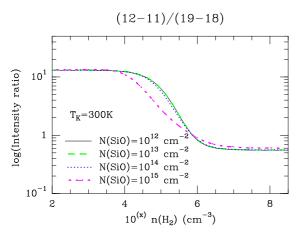


Fig. A.5. Same as A.4 but for T = 300 K.

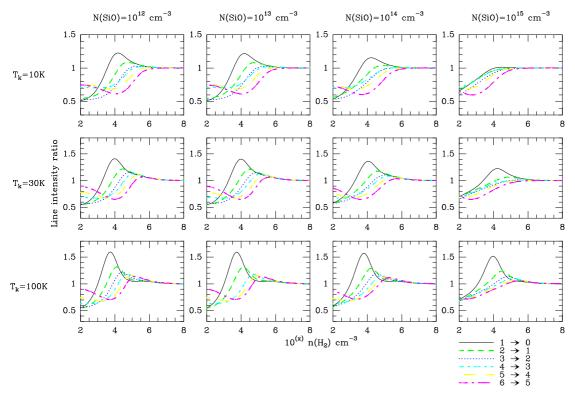


Fig. A.6. Same as A.3 for SiS with the SiS column density equal to 10^{12} , 10^{13} , 10^{14} and 10^{15} cm⁻².

Appendix B: Online Figures

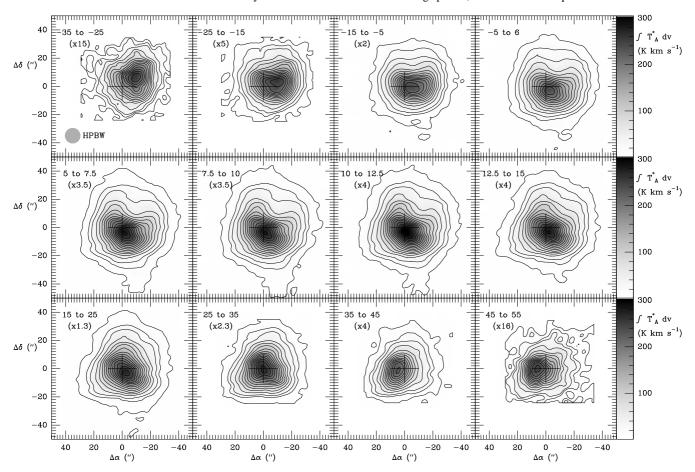


Fig. B.1. Integrated intensity of the J=5-4 transition of SiO at different velocity ranges (indicated at the top of each panel). In some panels, the integrated intensity of the maps has been multiplied by a scale factor (indicated in the panels) to maintain the same color dynamics for all maps. The step in integrated intensity ($\int T_A^* dv$) is 20 K km s⁻¹ from 25 to 305 K km s⁻¹ and the minimum contours are 5 and 15 K km s⁻¹. See text (Sect. 2) for main beam antenna temperature correction.

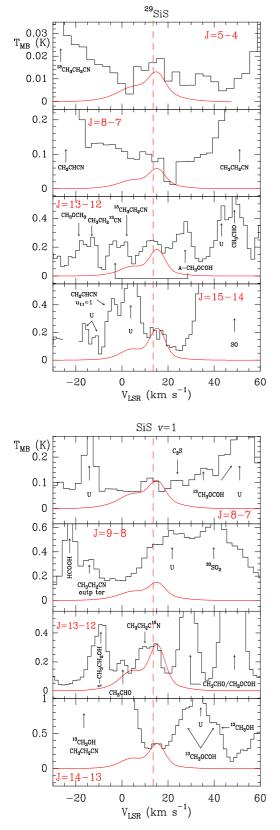


Fig. B.2. Observed lines (histogram spectra) and model (thin curves) of 29 SiS and SiS v=1. The dashed line shows a radial velocity at 13.5 km s⁻¹.

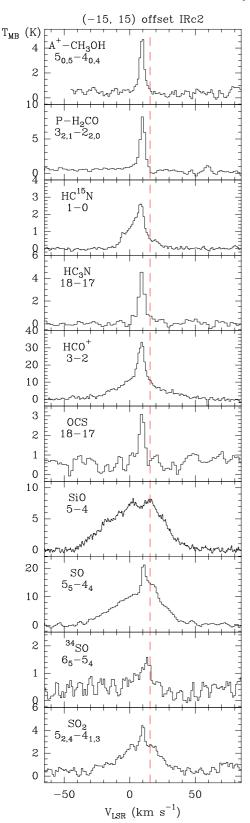


Fig. B.3. Observed lines of different molecules at a position (-15", 15") offset IRc2. The dashed line shows a radial velocity at 15.5 km s⁻¹.

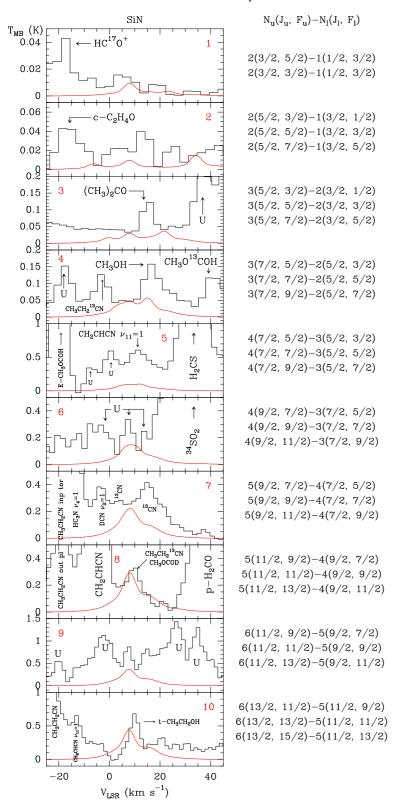


Fig. B.4. Observed lines (histogram spectra) and model (thin curves) of SiN.

Appendix C: Online Tables

Table C.1. SiO and SiO isotopologues velocity components.

Species	Wie	Wide component			Narrow component		
	v_{LSR} (km s ⁻¹)	$\Delta v (km s^{-1})$	$T_{MB}(K)$	$v_{LSR} \text{ (km s}^{-1}\text{)}$	$\Delta v (km s^{-1})$	$T_{MB}(K)$	
SiO 2-1	9.4±0.5	44±2	5.19	8.45±0.13	19.1±0.5	13.3	
SiO 3-2	10.2 ± 0.3	40.1 ± 0.9	15.5	8.4 ± 0.2	14.9 ± 0.7	10.8	
SiO 4-3	12.0 ± 0.3	41.7 ± 0.9	26.6	8.5 ± 0.2	15.8 ± 0.8	18.8	
SiO 5-4	11.91±0.13	40.4 ± 0.4	27.1	7.30 ± 0.11	14.8 ± 0.4	18.4	
SiO 6-5	9.7 ± 0.3	40.8 ± 0.5	46.1	7.7 ± 0.3	13.3 ± 0.8	15.6	
²⁹ SiO 4-3	7.9 ± 1.1	46±6	2.88	9.5 ± 0.3	15.5 ± 1.3	5.85	
³⁰ SiO 4-3				8.8 ± 0.2	19.7±0.5	5.15	
³⁰ SiO 5-4			•••	10.23 ± 0.15	21.0±0.6	6.19	
³⁰ SiO 6-5	7.8 ± 0.5	46±2	4.35	8.6 ± 0.2	16.8±0.7	8.50	

Notes. Velocity components of selected SiO and SiO isotopologues lines derived from two Gaussian fits.

Table C.2. SiS velocity components.

Species	Wide component			Narrow component			
	v_{LSR} (km s ⁻¹)	$\Delta v (km s^{-1})$	$T_{MB}(K)$	v_{LSR} (km s ⁻¹)	$\Delta v (km s^{-1})$	$T_{MB}(K)$	
SiS 6-5	8.8±0.5	24.0±0.9	0.39	15.4±0.3	7.0 ± 0.5	0.23	
SiS 8-7	9.6 ± 0.4	24.9 ± 1.0	1.03	15.7 ± 0.5	6.3 ± 1.0	0.49	
SiS 9-8	8.7 ± 0.4	24.6 ± 0.7	1.33	15.7±0.2	6.6 ± 0.5	1.15	
SiS 15-14	•••			15.7 ± 0.3	12.3±0.9	2.69	

Notes. Velocity components of selected SiS lines derived from Gaussian fits.

Table C.3. Molecular abundances

Region	Species	X (This work)	X^7	X^8	X^9
		$(\times 10^{-8})$	$(\times 10^{-8})$	$(\times 10^{-8})$	$(\times 10^{-8})$
Extended	SiO	0.05	< 0.05		
ridge ¹	SiS	•••			
Compact	SiO	0.20	0.80		
ridge ²	SiS	•••			
Plateau ³	SiO	2.20	0.80	1.10	23.5
	SiS	0.30			0.40
High velocity	SiO	2.20	•••	4.50	
plateau ⁴	SiS	•••			
Hot	SiO	0.20	0.60	•••	
core ⁵	SiS	0.30			
15.5 km s ⁻¹	SiO	1.00			
component ⁶	SiS	0.70		•••	

Notes. Derived molecular abundances and comparation with other works.
(1) Assuming $N(H_2)=7.5\times10^{22}$ cm⁻². (2) Assuming $N(H_2)=7.5\times10^{22}$ cm⁻². (3) Assuming $N(H_2)=2.1\times10^{23}$ cm⁻². (4) Assuming $N(H_2)=6.2\times10^{22}$ cm⁻². (5) Assuming $N(H_2)=4.2\times10^{23}$ cm⁻². (6) Assuming $N(H_2)=1.0\times10^{23}$ cm⁻². (7) From Sutton et al. (1995). (8) From Persson et al. (2007). (9) From Ziurys (1988).